# Comparative Structure Based Virtual Screening Utilizing Optimized AlphaFold Model Identifies Selective HDAC11 Inhibitor

Fady Baselious[1], Sebastian Hilscher[1], Dina Robaa[1], Cyril Barinka[2], Mike Schutkowski[3], Wolfgang Sippl[1]*

1 Department of Medicinal Chemistry, Institute of Pharmacy, Martin-Luther-University of Halle-Wittenberg, 06120 Halle (Saale), Germany

2 Institute of Biotechnology of the Czech Academy of Sciences, BIOCEV, 252 50 Vestec, Czech Republic

3 Charles Tanford Protein Center, Department of Enzymology, Institute of Biochemistry and Biotechnology, Martin-Luther-University of Halle-Wittenberg, 06120 Halle (Saale), Germany

## Abstract:

HDAC11 is a class IV histone deacylase with no crystal structure reported so far. The catalytic domain of HDAC11 shares low sequence identity with other HDAC isoforms which makes the conventional homology modeling less reliable. AlphaFold is a neural network machine learning approach that can predict the 3D structure of proteins with high accuracy even in absence of similar structures. However the fact that AlphaFold models are predicted in absence of small molecules and ions/cofactors complicate their utilization for drug design. Previously we optimized an HDAC11 AlphaFold model by adding the catalytic zinc ion and minimization in the presence of reported HDAC11 inhibitors. In the current study we implement a comparative structure-based virtual screening approach utilizing the previously optimized HDAC11 AlphaFold model to identify novel and selective HDAC11 inhibitors. The stepwise virtual screening approach was successful in identifying a hit that was subsequently tested using an in vitro enzymatic assay. The hit compound showed an $IC_{50}$ value of 3.5 µM for HDAC11 and could selectively inhibit HDAC11 over other HDAC subtypes at 10 µM concentration. In addition we carried out molecular dynamics simulations to further confirm the binding hypothesis obtained by the docking study. These results reinforce the previously presented AlphaFold optimization approach and confirm the applicability of AlphaFold models in the search for novel inhibitors for drug discovery.

## Keywords:

AlphaFold; HDAC11; virtual screening; modelling; in vitro assay; pharmacophore; docking; molecular dynamics simulation

# 1-Introduction:

HDAC11, the sole member of class IV of HDACs family, is the smallest member of the family and one of the least studied HDAC subtypes [1, 2]. It was demonstrated that HDAC11 is involved in various physiological and pathological processes [3-5] and represents a potential target for the treatment of several diseases including multiple sclerosis, viral infections and obesity-related diseases [6-8]. HDAC11 was also found to be involved in the modulation of cancer growth and is overexpressed in different cancer forms [9-16]. For example, inhibition of HDAC11 showed beneficial effects in neuroblastoma cells [17] suggesting that HDAC11 represents a promising target for the treatment of some cancer forms.

No crystal structure of HDAC11 has been reported and its catalytic domain shows low sequence identity (<30%) when compared to the primary sequences of the catalytic domains available in the PDB databank for other human HDAC isoforms. This fact complicates the conventional template-based homology modeling [18].

AlphaFold is a neural network machine learning approach for predicting the 3D structures of proteins with atomic accuracy even in absence of known similar structures [19]. The database of the 3D structures of the whole human proteome was constructed by AlphaFold [20]. The models from AlphaFold should be carefully considered when used for structure-based drug design studies because the folding is predicted in absence of small molecules like water molecules, ligands and cofactors.

In a recent study by Ren et al. [21] AI driven molecular generation was combined with utilization of AlphaFold model for the aim of drug discovery for cyclin dependent kinase 20 (CDK20). In this study, modification of the AlphaFold model by removing the C-terminus which was blocking the solvent exposed region of the protein and occupying the ATP binding pocket through Arg305 was performed in order to make the model usable. In another study, Zhu et al. [22] utilized a similar approach to successfully design new inhibitors for salt inducible kinase 2 (SIK2).

The two studies discussed above used AlphaFold models for protein targets sharing reliable sequence identity with other proteins within the same family for which crystal structures are available and utilized AI driven molecular generation techniques rather than docking. Several other studies addressed the usability of AlphaFold models for docking [23-27] and real world virtual screening scenarios [25, 28, 29]. One of these studies assessed the usability of AlphaFold structures predicted while excluding structural templates with more than 30% identity thus imitating virtual screening process with a model based on low prior structural information. Results from these studies demonstrated a worse performance of the AlphaFold models compared to crystal structures suggesting that using unmodified AlphaFold models is not an ideal scenario. This worse performance could be due to the collapse or distortion of the binding site

resulting from minor variation at the side chain level or larger variation of the backbone, suggesting post-modeling or optimization is required to obtain more realistic holo models [24-29].

In agreement with these results, it was demonstrated that optimization of the binding site by inducing flexibility or manual modification of the low confidence regions could enhance the docking results [23, 25, 26, 30]. In our recent work, we showed that binding site optimization of HDAC11 AlphaFold model by adding the catalytic zinc ion and performing minimization in the presence of transplanted ligands resulted in a model that could be used for docking of the known selective HDAC11 inhibitors FT895, MIR002 and SIS17 [18].

In the current study, we present an application for using optimized AlphaFold models for virtual screening while addressing HDAC subtype selectivity. We demonstrate herein, that our previously optimized HDAC11 AlphaFold model was successfully utilized for picking a selective hit through comparative virtual screening approach. In the developed multistep screening, various approaches including structure based pharmacophore screening, ligand docking, pose filtering and prioritization were applied as described in the Methods section. To experimentally confirm the virtual screening results the most promising hit was synthesized and tested in vitro using different HDAC subtypes. In addition, we analyzed the predicted binding mode from docking by means of molecular dynamics (MD) simulations.

## 2-Materials and Methods:

Schrödinger Suite 2019 was used for all of the modeling work. Maestro [31] was utilized for visualization.

### 2.1-Protein preparation:

All protein structures were preprocessed using Protein Preparation Wizard [32, 33] by adding hydrogen atoms and assigning bond orders. Zero order bonds to metals were created and water beyond 5 Å from the ligands was deleted. Filling in missing side chains and loops using Prime [34-36] was performed. Ionization states of the ligands were generated using Epik [37-39] at pH 7.0 ±2.0. The deprotonated hydroxamates form was selected for further hydrogen bond optimization. Hydrogen bond optimization was assigned with sampling water orientation and using PROPKA at pH 7.0.

### 2.2-Grid generation:

For all protein-ligand complexes, grids were generated using the Receptor Grid Generation panel and utilizing the centroid of the ligand as the center of the grid.

### 2.3-Ligand preparation:

Ligands were prepared in the predominant form at pH 7 utilizing the LigPrep [40] panel with OPLS3e force fields.

## 2.4-Data base acquiring and curation:

### 2.4.1-Acquiring ligand database:

A focused library of benzohydroxamic acids (SMARTS= C1=CC=C(C(=O)NO)C=C1) comprising 407834 ligands was downloaded from https://tldr.docking.org/ using the zinc20-all database [41].

### 2.4.2-Ligand preparation:

The library was prepared using Ligprep and resulted in 510529 structures using OPLS2005 [42-45] with generating possible states at pH 7.2 ± 2 using Epik. Specified chiralities from the original dataset were retained.

### 2.4.3-Properties calculation:

The rule of five property was calculated for all ligands in the database using QikProp [46] properties from the Molecular Descriptor panel.

### 2.4.4-Database filtering:

The prepared library was filtered to select the hydroxamate form of the ligands using a defined custom pattern of [O-]N([H])C(=O)c1ccccc1. The library was filtered using the calculated rule of five property thereby discarding all structures which showed one or more violations for the rule of five using the Ligand Filtering panel. 18113 compounds could successfully pass the aforementioned filters.

## 2.5-Virtual screening:

### 2.5.1-Structure based pharmacophore modeling:

#### 2.5.1.1-Pharmacophore generation:

The E-pharmacophore [47, 48] hypothesis was generated using the Develop Pharmacophore Model panel form Schrödinger Phase [49-51] utilizing the optimized AlphaFold TSA-HDAC11 complex with the flipped-out Phe152 rotamer [18]. The auto E-pharmacophore method was used to specify the maximum number of features to be generated and assign the receptor-based excluded volume shell.

#### 2.5.1.2-Pharmacophore screening:

The prepared database was screened through Phase Ligand Screening panel using the previously generated E-pharmacophore and implementing the four obtained features and excluded volumes. Up to 50 conformers were generated during the search and specifying to report at most one hit per ligand. 12154 hits could successfully pass the pharmacophore screening.

### 2.5.2-Docking into HDAC11 AlphaFold model:

The hits obtained from the pharmacophore screening were docked into the HDAC11 AlphaFold model using Glide [52-55] with standard precision and flexible ligand sampling. 15 poses were subjected to post docking minimization and reporting the top scored pose. 12151 compounds could be successfully docked.

### 2.5.3-Pose filtering:

The obtained docking poses in the HDAC11 AlphaFold model were filtered using Pose Filter panel utilizing the distance between the carbonyl and the hydroxyl oxygens of the hydroxamate moiety and the zinc ion while specifying contact maximum distance to be 2.6 Å. 11409 poses could successfully pass the filter.

### 2.5.4-Docking and pose filtering in other HDACs isoforms:

#### 2.5.4.1-Validation by re-docking of the native ligand

To validate the docking protocol, re-docking of the co-crystallized ligands of HDAC1 (PDB 5ICN), HDAC6 (PDB 5EDU) and HDA8 (PDB 5FCW) was performed and RMSD for the docked and the native poses was calculated. RMSD was found to be 2.018 Å, 1.192 Å and 0.416 Å for HDAC1, HDAC6 and HDAC8 respectively.

#### 2.5.4.2-Docking and pose filtering

The filtered poses from the HDAC11 docking results were further docked into HDAC1, HDAC6 and HDAC8. The obtained docking poses were further subjected to Pose Filter. Ligand docking and pose filtering were performed using the same settings as mentioned for HDAC11. 450, 9934 and 11308 hits could be successfully docked to HDAC1, HDAC6 and HDAC8 respectively. Compounds that could show correct poses and zinc chelation in HDAC1, HDAC6 and HDAC8 were removed from the final HDAC11 inhibitor hit list.

### 2.6-REOS filtering and MM-GBSA calculations:

To remove compounds with reactive groups that may interfere with biological evaluation, rapid elimination of swill (REOS) filter was applied using structure filter in Canvas [56-58].

To prioritize the hits for further evaluation, ligand binding energies were calculated using the molecular mechanics with generalized Born and surface area solvation (MM-GBSA). For this purpose, the Prime MM-GBSA panel was utilized with specifying the variable-dielectric generalized Born (VSGB) solvation model, sampling by minimizing all atoms using OPLS3e force field.

### 2.7-Molecular dynamics simulation:

The predicted binding mode of the virtual screening hit of HDAC11 was further analyzed by means of molecular dynamics simulation using program Desmond [59, 60]. The HDAC11-inhibitor complex was

simulated for 50 ns and the simulation was repeated three times applying different random seeds. Furthermore, a single longtime scale MD run was performed for 500 ns. The system was solvated in SPC water model using an orthorhombic box and 10 Å distance between the solute structures and the simulation box boundary. The box volume was then minimized. The system was neutralized by adding chloride ions that were placed 4 Å away from the ligand.

The prepared system was relaxed using the default Desmond relaxation protocol for NPT ensemble followed by a production run utilizing the NPT ensemble at the temperature of 300 K using a Nose–Hoover chain thermostat and a pressure of 1.01325 bar using Martyna-Tobias-Klein barostat. The progress of the simulation was recorded every 100 ps.

For analysis, the Simulation Event Analysis panel was used for RMSD and distance calculations. The RMSD of the protein was calculated using the backbone atoms while the RMSD of the ligand and the zinc ion was calculated by fitting to the protein backbone. The Simulation Interaction Diagram panel was used for analyzing the RMSF and the interaction persistence of the ligands. RMSD of the protein was calculated excluding the termini (residues: 1-14 and 321-347).

## 2.8-In vitro enzymatic inhibition evaluation:

Full-length human HDAC11 was expressed and purified as described previously [61]. A fluorescence based HDAC11 assay was used. The fluorescence measurements were performed using a PerkinElmer Envision 2104 multilabel plate reader (Waltham, MA, USA) at $\lambda_{ex}$ = 320 nm and $\lambda_{em}$ = 430 nm. The reaction mixture consisted of HDAC11, and the substrate in a reaction buffer comprising 50 mM HEPES, 2 mg/mL BSA, and 70 μMTCEP, and at pH 7.4 which was adjusted with NaOH (total volume 40 μL). The reactions were incubated in black 384-well plates for 30 min (scan every 30 s) at room temperature, and the increase of relative fluorescence reflecting the product formation was monitored. Positive and negative controls were included in every measurement. They were set as 100 and 0 % respectively and the measured values were normalized accordingly.

Recombinant human HDAC1 and HDAC6 were purchased from ENZO Life Sciences AG (Lausen, CH) whereas HDAC8 was produced as described before [62]. In vitro testing of the inhibitors in an enzymatic assay was carried out as described in previous publications [62, 63]. For HDAC1 a substrate peptide derived from p53 (Ac-RHKK(Acetyl)-AMC) was used. For HDAC6, the substrate (Abz-SRGGK(thio-TFA)FFRR-NH$_2$) was used as described before [62]. The enzyme inhibition of HDAC8 was determined with a homogenous fluorescence assay and the substrate Fluor-de-Lys as described before [63]. All measurements were performed in assay buffer (50 mM HEPES, 150 mM NaCl, 5 mM MgCl$_2$, 1 mM TCEP and 0.2 mg/mL BSA, pH 7.4 adjusted with NaOH) at 37 °C. An Envision 2104 Multilabel Plate Reader (PerkinElmer, Waltham, MA), with an excitation wavelength of 380 ± 8 nm (320 ± 8 nm for

HDAC8) and an emission wavelength of $430 \pm 8$ nm was used to measure the fluorescence intensity. Positive and negative controls were included in every measurement and were set as 100 and 0 %, respectively and the measured values were normalized accordingly.

## 3-Results and Discussion:

### 3.1-Dataset selection and curation:

Hydroxamates comprise well defined and characterized pharmacophore for HDAC inhibitors and considered the most commonly used zinc binding group in HDAC inhibitors [64, 65]. Some of the inhibitors bearing the hydroxamate scaffold as vorinostat (SAHA), belinostat (PXD-101) and panobinostat (LBH589) are already approved by FDA for treatment of hematological malignancies [66]. Benzohydroxamates constitute an important class of HDAC inhibitors and their development entail an active field within inhibitors design for several HDAC subtypes [65]. ZINC20 is a publicly available database that includes nearly two billion compounds in 2D and 3D downloadable formats through a website that allows for rapid analogue search [41]. Initially, a focused database of 407834 benzohydroxamates was acquired from the ZINC20 database. The library was further prepared with generating possible ionization states at physiological pH $7.0 \pm 2.0$. The preparation step resulted in library that contained 510529 ligands with various ionization states which was then subjected to filtration to select the ligands with hydroxamate state only. The Lipinski rule of five is an important early measure for identifying bioavailable drug like candidates. According to this rule the compound must possesses the following properties: molecular weight <500 Da, logP <5, H-bond donors <5, and H-bond acceptors <10. To further select drug like molecules the prepared library was filtered to remove any molecule that violate Lipinski's rule of five [67, 68]. The initial curation resulted in a library of 18,113 ligands. The multistep virtual screening process was the performed as presented in the workflow (**Fig. 1**).
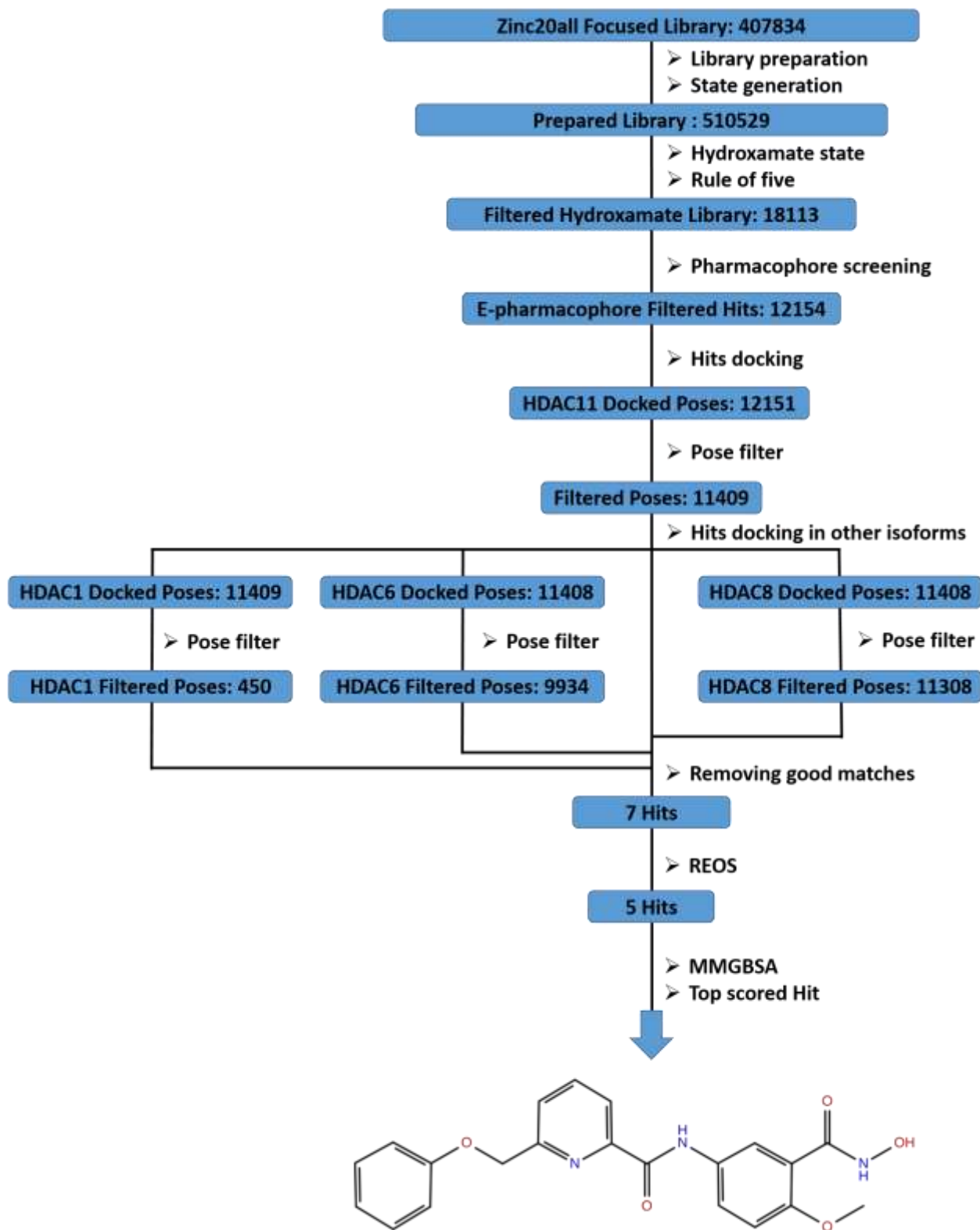
**Fig. 1**. Workflow of the stepwise virtual screening.

## 3.2-Virtual screening:

The E-pharmacophore module implemented in Phase automatically generates a pharmacophore hypothesis that is based on the complementarity of the protein and ligand features from a protein-ligand complex. This involves using Glide XP scoring terms to determine which features contribute the most to the binding. The hypothesis obtained from using the previously optimized complex of TSA and HDAC11 AlphaFold model exhibited four features (**Fig. 2)**, namely a hydrogen bond acceptor feature assigned for the carbonyl-O, a hydrogen bond donor assigned to the NH and negative feature for the deprotonated hydroxyl group of the hydroxamate zinc binding group as well as an aromatic feature for the phenyl capping group. Excluded volumes that are based on the occupation of space by protein atoms were also added. The preliminary screening was performed to select the ligands which match the four features with the aim of filtering out very small ligands and fragments thus retaining only ligands with suitable size for the docking-based virtual screening.
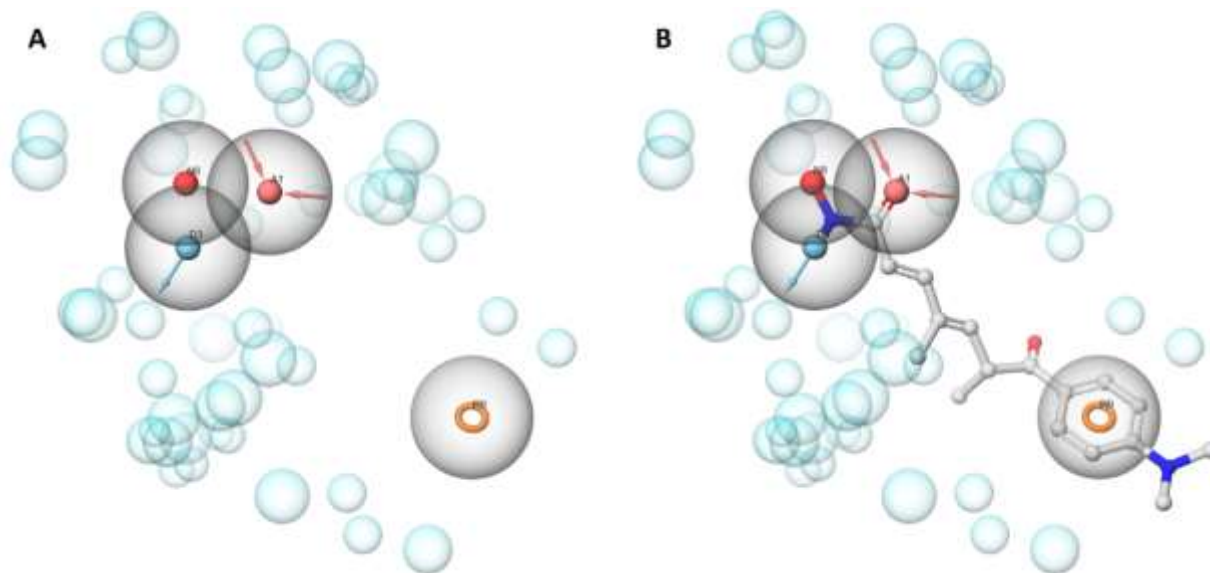


**Fig. 2**. E-pharmacophore model. **A**, pharmacophore features: HB donor represented as cyan sphere, HB acceptor as pink sphere, negative as red sphere and aromatic as orange ring. Excluded volumes are represented as cyan transparent spheres and feature matching tolerance as grey transparent spheres. **B**, superposition of the inhibitor TSA on the features of the generated hypothesis. Ligand is represented as grey sticks.

The pharmacophore screening step was effective and could filter out 5959 compounds. Docking-based virtual screening of the remaining 12154 structures was then performed using the grid generated from the HDAC11-TSA optimized AlphaFold model. In our previous study, we were successful to obtain four optimized complexes by minimization of the HDAC11 AlphaFold model with previously reported active ligands of HDAC11 for which X-ray crystal structures with HDAC8 are available in the protein data bank (PDB). The selection of the TSA-HDAC11 complex for the virtual screening was based on the results

obtained from the previous study since it showed the best performance regarding the docking of the selective inhibitor FT895 (**Fig. 3)** and was further utilized in docking of other selective inhibitors as MIR002 and SIS17. Almost all of the hits from the pharmacophore screening step could pass the docking based screening. Furthermore, filtration of the obtained docking poses was performed to select the ligands that can show a bidentate chelation mode to the catalytic zinc ion. Pose filtration was performed utilizing the distances between the chelator carbonyl and hydroxyl oxygen atoms of the hydroxamate moiety to the zinc ion. Compounds showing distances more than a cut off of 2.6 Å between any of the chelator atoms and the zinc ion were removed.
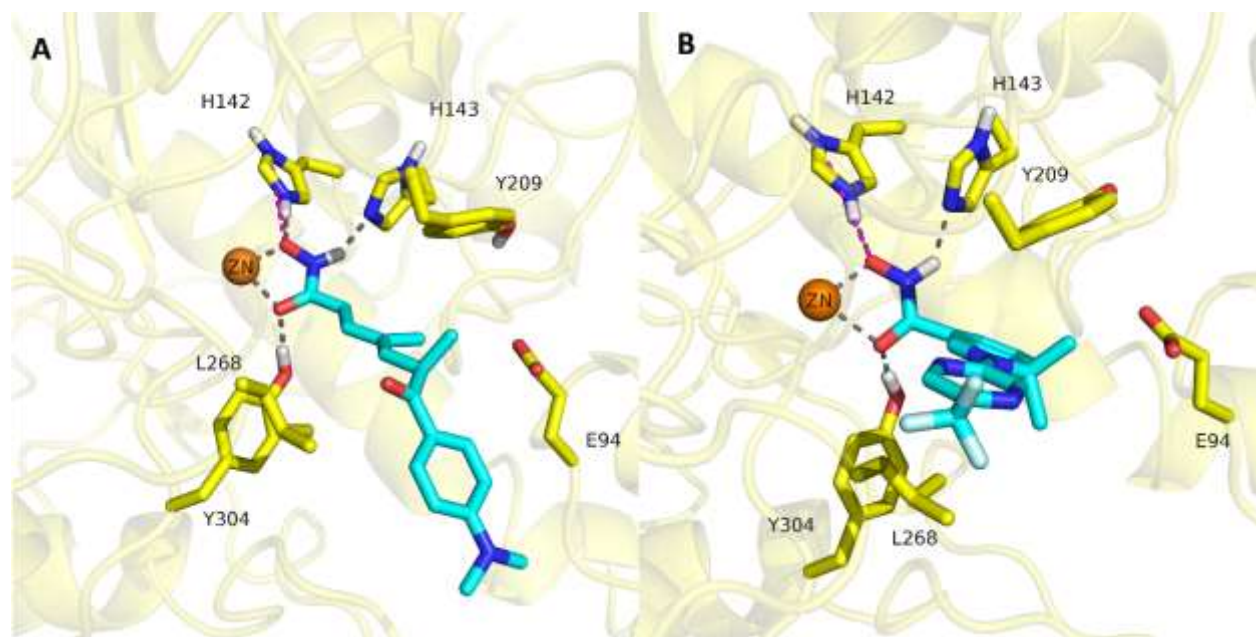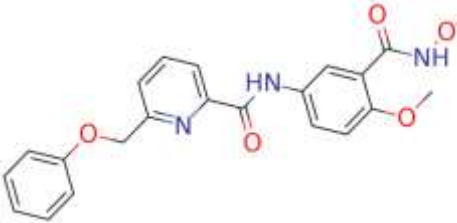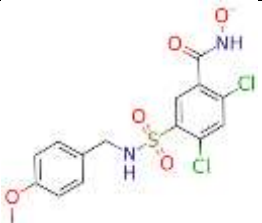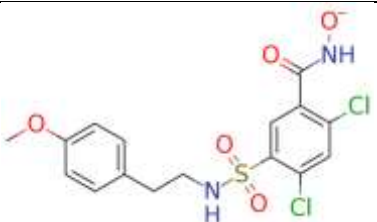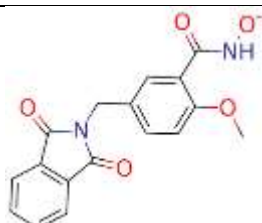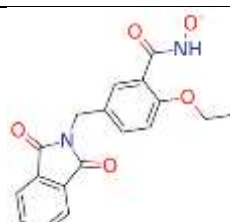


**Fig. 3A**. Minimized pose of TSA in HDAC11 optimized AlphaFold model. **B**. Docked pose of FT895 in the optimized HDAC11 AlphaFold model. The protein backbone is represented as yellow cartoon, the interacting binding site residues as yellow sticks, zinc ion as orange sphere and the ligands as cyan sticks. Hydrogen bonds and coordination bonds are represented as grey dashed lines and ionic interactions as magenta dashed lines.

For the aim of searching for selective HDAC11 ligands, a comparative docking-based virtual screening approach was then applied. The hits obtained from the docking in HDAC11 which could pass the pose filtration step were then screened by docking into HDAC1, HDAC6 and HDAC8 crystal structures. The obtained hits from every screening were further subjected to pose filter screening. Ligands which could show correct docking pose with bidentate chelation of the catalytic zinc ion in any of HDAC1, HDAC6 and HDAC8 were removed from the HDAC11 hit list. For HDAC6, ligands which could chelate the zinc ion in a monodentate fashion were also removed. This step was very effective and could filter out most of

the compounds leaving only 7 compounds (**Table S1**) that could show a correct chelation mode in HDAC11 but not in any of the other isoforms.

Rapid elimination of swill (REOS) [69, 70] filter was then applied to remove compounds containing reactive or toxic moieties which might also interfere with biological assays. Two compounds containing nitro groups were removed by using this filter. Interestingly, the final five hits (**Table. 1**) are all bearing a methoxy, ethoxy or chloro substituent on the ortho position of the hydroxamate moiety which indicates that substitution at this position might represent a selectivity determinant for HDAC11 inhibition.

**Table 1:** Final hits and MM-GBSA dG binding values.

| ID | Title | Structure | MM-GBSA dG bind |
|----|-------|-----------|-----------------|
| **1** | ZINC000028464438 | | -49.76 |
| **2** | ZINC000671998736 | | -39.75 |
| **3** | ZINC000742823399 | | -48.68 |
| **4** | ZINC000916666211 | | -48.21 |
| **5** | ZINC000916666264 | | -41.45 |

In the last step of the virtual screening workflow the five final hits were prioritized through MM-GBSA calculations. MM-GBSA calculations showed that the top ranked molecule is ZINC000028464438 (**1**) which is bearing a methoxy group as ortho substitution to the hydroxamate moiety and an amide linker in the meta-position. It is worth noting that a selective HDAC11 inhibitor (PB94) was recently presented by Bai et al. [71]. Based on the structure activity relationship, the authors reported that a methoxy group in the ortho position of their developed benzohydroxamate inhibitors is a key factor for HDAC11 selectivity which is in agreement with our results from the virtual screening.

### 3.3-In Vitro enzymatic evaluation:

Due to the unavailability of the top-ranked hit ZINC000028464438 (**1**) we decided to resynthesize the compound as reported [72], purified it, confirmed the structure by NMR and MS and tested it at a concentration of 10 μM against HDAC11 as well as HDAC1, HDAC6 and HDAC8 as representatives for class I and class II HDACs to determine the selectivity (Synthesis and analytical characterization described in detail in the Supplement). Compound **1** showed inhibition of the enzymatic activity of around 85 % for HDAC11 while it showed almost no inhibition for HDAC1 and HDAC8 and only around 20 % inhibition of HDAC6 (**Fig. 4A**). Interestingly, the findings from the in vitro screening confirms the results obtained from the theoretical study as the hit compound was not able to adopt reasonable poses in any of HDAC1, HDAC6 and HDAC8. On the other hand, a perfect pose with bidentate chelation mode that was also showing the expected interactions of a benzohydroxamate based HDACs inhibitor was observed in HDAC11 and proved to be stable during MD simulations. These results further confirm that HDAC11 can accommodate such bulkier substitutions in the ortho position of the benzohydroxamate moiety of the inhibitor providing a unique feature that can be used to target isoform selectivity when designing new inhibitors.

Furthermore, the $IC_{50}$ for HDAC11 was determined to be about 3.5 μM (**Fig. 4B**). While this virtual screening hit showed only moderate HDAC11 inhibitory activity, it still can be considered a promising hit compound due to the good selectivity. Further chemical optimization is required that might include manipulation of the size and structure of the ortho substituent at the benzohydroxamate moiety, changing the position and structure of the amide linker or changing the structure and decorations of the capping group. The obtained results can be assessed in the light of capabilities of virtual screening and the role it plays for hit identification and finding new scaffold leads by screening of large compound libraries, a process that is commonly followed by lead optimization.
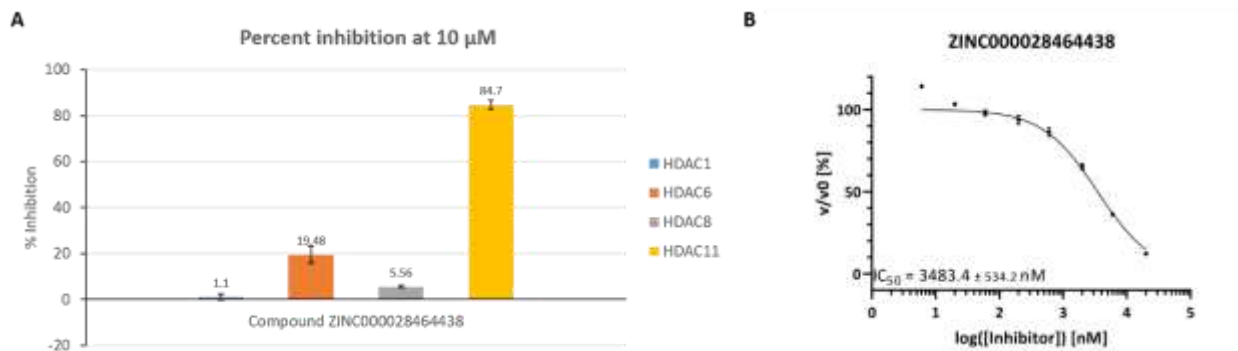
**Fig. 4A**. Relative inhibition of enzymatic activity for different HDAC isoforms at 10 µM of ZINC000028464438 (**1**). **B**. Determination of IC$_{50}$ value of ZINC000028464438 (**1**) for HDAC11.

## 3.4-Analysis of the docked poses:

Analyzing the docked poses of the confirmed hit revealed that the obtained pose of the hit compound in the optimized HDAC11 AlphaFold model (**Fig. 5**) showed bidentate chelation with distances of 2.41 Å and 2.17 Å between the zinc ion and the carbonyl and hydroxyl oxygen atoms of the hydroxamate moiety, respectively. A salt bridge to His142 as well as hydrogen bond interactions with His143 and Tyr304 were observed. The ligand also demonstrated $\pi-\pi$ interactions between the phenyl ring of the benzohydroxamate and His183. The phenoxymethyl capping group adopts a bent conformation and is directed towards loop1. For HDAC1 the hit ligand showed a pose in which no metal chelation was observed as the hydroxamate moiety could not reach the zinc ion in the depth of the binding pocket but barely reaching to His178 with which the ligand forms hydrogen bond through the hydroxyl oxygen of the hydroxamate moiety. Another hydrogen bond was observed between the NH of the amide linker and Asp99 side chain. In HDAC6, the docking resulted in a flipped orientation with the hydroxamate moiety facing the solvent which indicates that the ligand could not fit into the binding site. No interactions could be observed for the obtained pose in HDAC6. The hit ligand could not show the bidentate zinc chelation commonly observed for cocrystallized HDAC8 inhibitors.
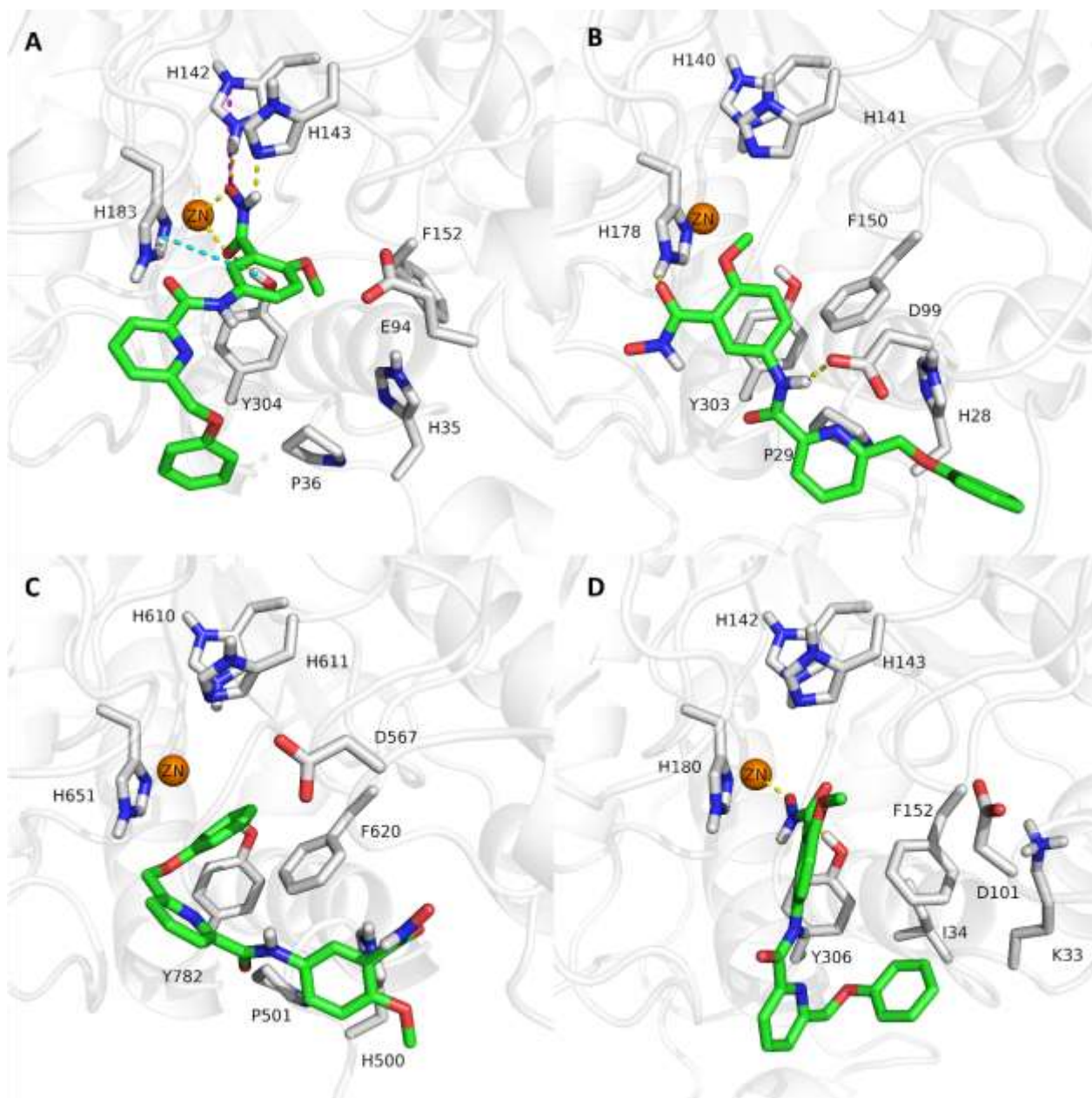
**Fig. 5**. Docked poses of ZINC000028464438 (**1**). **A**. HDAC11. **B**. HDAC1. **C**. HDAC6. **D**. HDAC8. The protein backbone is represented as white cartoon, the interacting binding site residues as grey sticks, zinc ion as orange sphere and the ligands as green sticks. Hydrogen bonds and coordination bonds are represented as yellow dashed lines, π –π interactions as cyan dashed lines and the ionic interactions as magenta dashed lines.

## 3.5-Molecular dynamics simulations:

Docking methods are limited by not considering the flexibility of the protein but treating the receptor as rigid body. On the other hand, MD simulation technique takes into account the flexibility of the complex thus giving a deeper insight regarding the binding mode of the ligand and its behavior in dynamic

environment. Therefore we decided to study the binding mode of the confirmed hit extensively using short and long MD simulations. The docking pose of the hit compound in the optimized HDAC11 AlphaFold model was subjected to three short (50 ns) molecular dynamics simulations using different random seeds. Furthermore, a longer MD simulation (500 ns) was performed to assess the stability of the obtained pose over a longer time scale.

In all MD simulations the protein and the zinc ion demonstrated high stability that could be observed through the calculated RMSD plots. The protein backbone is stabilizing between 1 Å and 2 Å while the zinc ion is stabilizing almost at 1 Å (**Fig. 6A** and **6B**).

The results of the three independent short MD simulations were comparable. The RMSD plot of the ligand demonstrated that there is a shift in the pose directly after the simulation started and that the ligand is stabilizing between 3 Å and 4 Å till the end of the simulation (**Fig. 6C**). Analyzing the RMSF of the ligand heavy atoms showed that the phenoxymethyl capping group is the most fluctuating substructure of the ligand and with an RMSF reaching 2 Å (**Fig. 6D**).
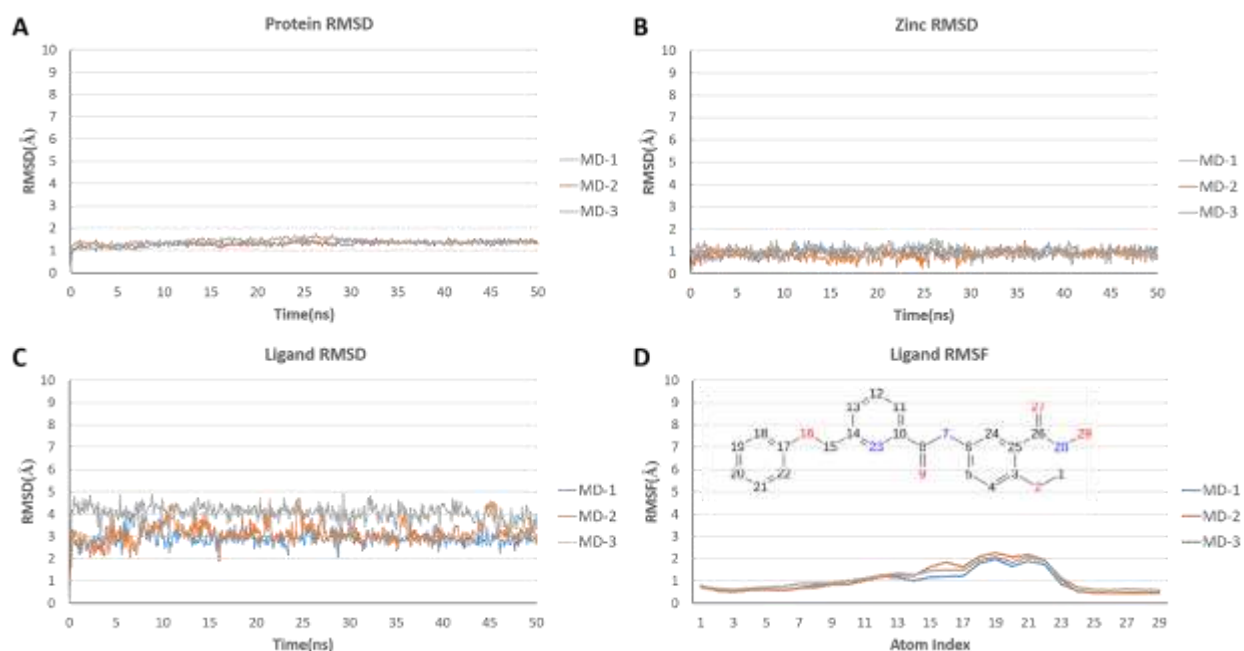


**Fig. 6**. RMSD and RMSF plots of ZINC000028464438 (**1**) for 3 repeated MD runs each for 50 ns. **A**, RMSD plots of protein backbone heavy atoms. **B**. RMSD plots of zinc ion. **C**. RMSD plots of ligand heavy atoms. **D**. RMSF plots of ligand heavy atoms.

Inspecting the MD trajectories showed that there is a slight shift of the initial docking pose allowing for the benzohydroxamate moiety to be accommodated deeper into the binding pocket which leads also to a better accommodation of the capping group through the relaxation of the conformation (**Fig. 7C**).

The stability of the bidentate chelation mode was confirmed for the three runs by monitoring the distances between the chelator atoms of the hydroxamate zinc binding group and the zinc ion (**Fig. 7A** and **7B**). The salt bridge to His142 showed very high stability with persistence of almost 100% for the three runs. The hydrogen bond interaction to His143 showed moderate stability with persistence ranging between 54% and 72%. It is worth noting that we observed such week to moderate stability of the hydrogen bond interaction to His143 during MD simulation with some of the ligands we utilized for the model optimization in our previous study as TSA and also with some of the selective docked ligands as FT895 and MIR002 [18]. The slight shift in the pose discussed above leads to almost complete loss of the hydrogen bond between Tyr304 and the carbonyl oxygen of the hydroxamate moiety but allowed for the formation of another hydrogen bond between the same residue and the oxygen of the methoxy substituent in the ortho position of the benzohydroxamate substructure that showed high stability with persistence ranging between 72% and 87%. This shift in the pose also allowed for the formation of another hydrogen bond interaction that was not observed in the initial docked pose between His183 and carbonyl oxygen of the amide linker, however, low stability of this interaction was observed with persistence between 26% and 37%. (**Table S2** and **Fig. 10 and 11**).
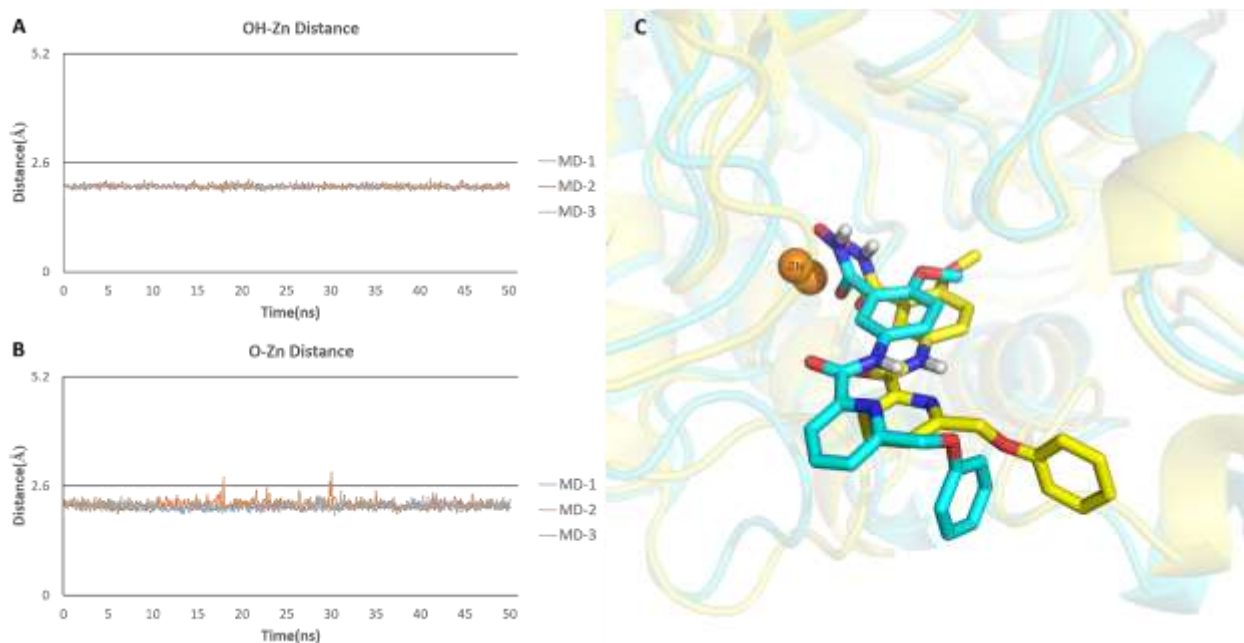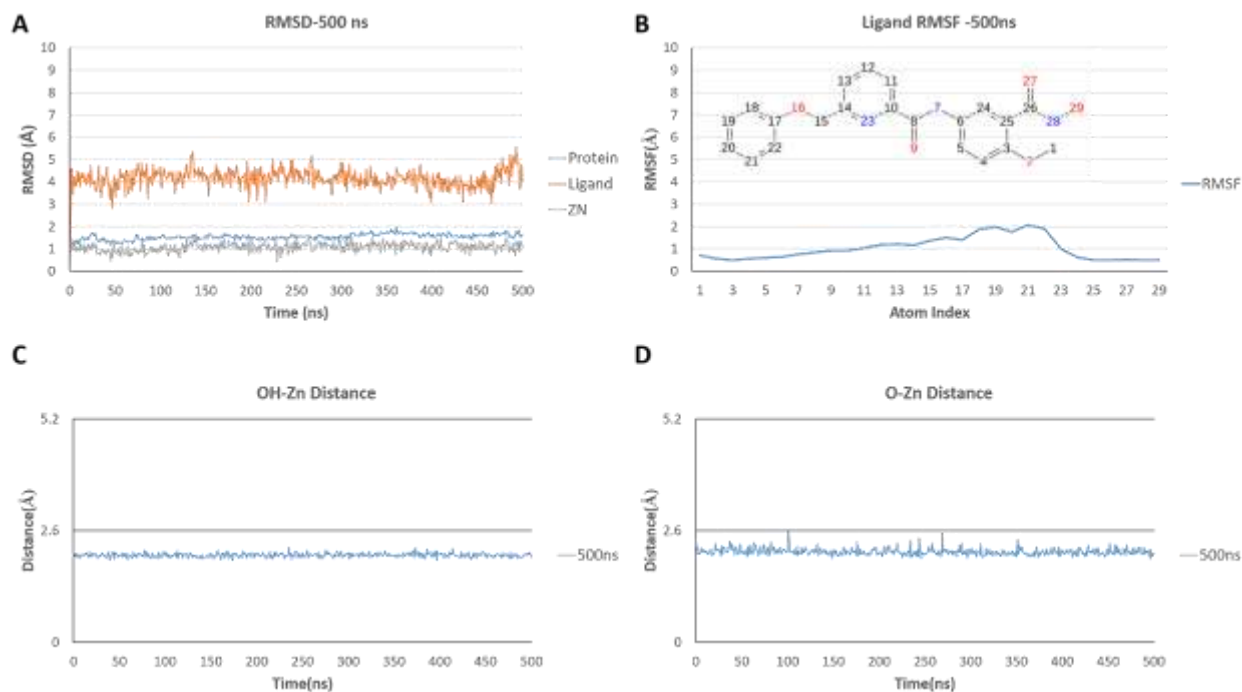


**Fig. 7A** and **B.** Distances to the zinc ion for three repeated MD runs each for 50 ns for the hydroxyl and the carbonyl oxygen atoms of the hydroxamate zinc binding group, respectively. **C.** Superposition of the first and last frames of ZINC000028464438 (**1**) showing the shift in the pose during the simulation from the first MD run of 50 ns. The zinc ion is represented as orange sphere, the protein backbone as cartoon and ligand as sticks. The protein backbone and the ligand are colored in cyan and yellow for the first and last frames, respectively

The longer molecular dynamics simulation could confirm the stability of the obtained pose of the hit in the HDAC11 AlphaFold model in a long time scale. Inspecting the RMSD plot of the ligand showed that it is

stabilizing between 4 Å and 5 Å (**Fig. 8A**) with the RMSF indicating that the most fluctuating substructure is the phenoxymethyl group (**Fig. 8B**). Distances between the zinc ion and the chelator atoms of the hydroxamate zinc binding group showed to be stable thus confirming the bidentate chelation mode (**Fig. 8C** and **8D**).



**Fig. 8A**. RMSD plots of the protein backbone heavy atoms, zinc ion and ligand heavy atoms for the long MD run (500 ns). **B**. RMSF plots of the ligand, ZINC000028464438 (**1**) heavy atom for the long MD run (500 ns). **C** and **D**. Distances to the zinc ion for the hydroxyl and the carbonyl oxygen atoms of the hydroxamate zinc binding group, respectively, for the long MD run (500 ns).

MD simulation trajectory analysis demonstrated the same slight shift in the pose with the benzohydroxamate moiety inserted deeper into the binding pocket along with the relaxation of the phenoxymethyl capping group (**Fig. 9**) as observed in the three independent shorter MD runs.
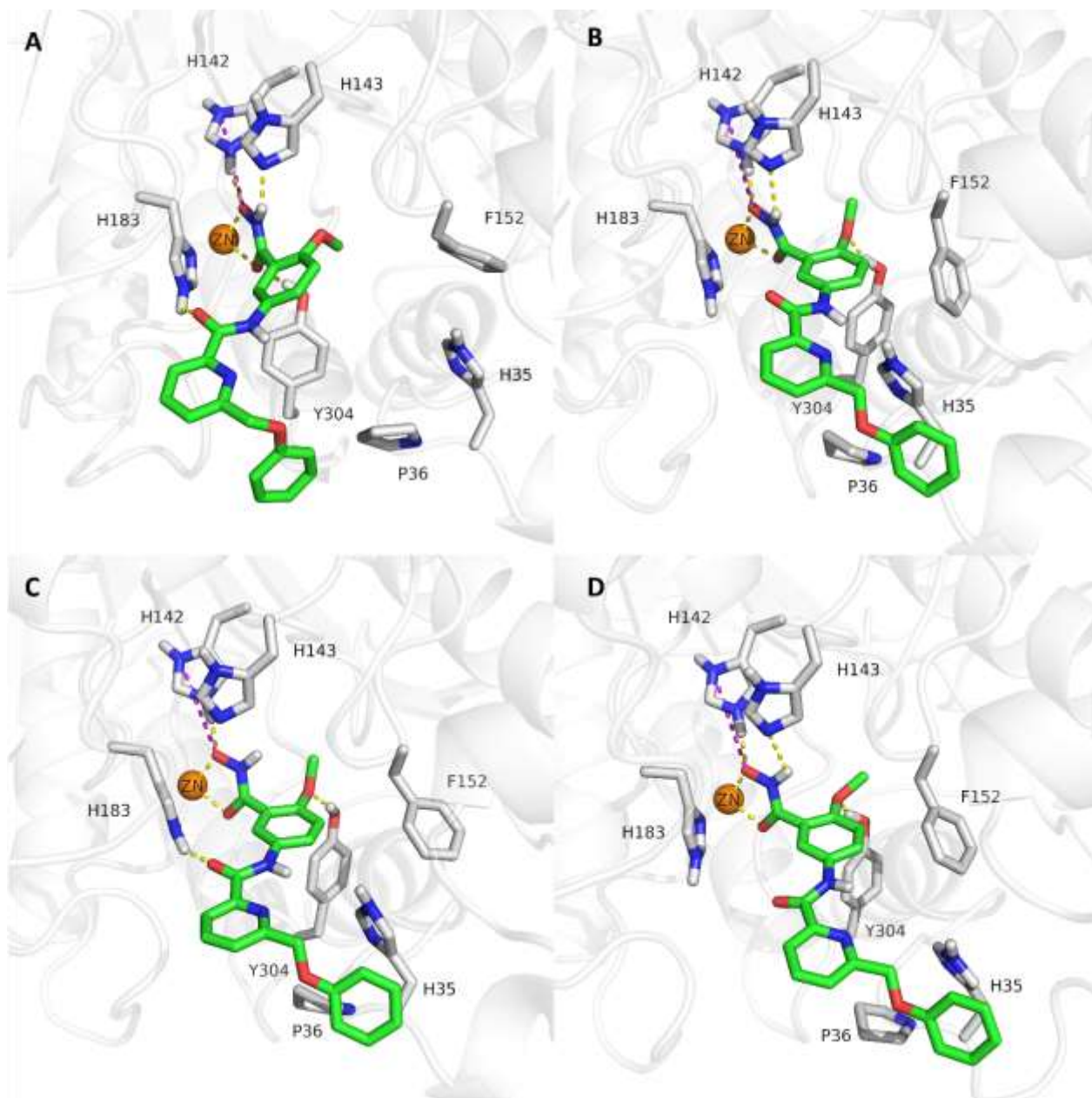
**Fig. 9**. Selected snapshots from the long MD simulation (500 ns) of ZINC000028464438 (**1**)-HDAC11 docked pose showing the shift in the pose and fluctuation of the phenoxymethyl capping group. **A**. Frame 1. **B**. Frame 1250. **C**. Frame 2500. **D**. Frame 5000. The protein backbone is represented as white cartoon, the interacting binding site residues as grey sticks, zinc ion as orange sphere and the ligands as green sticks. Hydrogen bonds and coordination bonds are represented as yellow dashed lines and the ionic interactions as magenta dashed lines.

The salt bridge between the deprotonated hydroxyl oxygen of the zinc binding group and His142 showed very high stability with persistence of about 100% while for His143 the hydrogen bond interaction with the carbonyl oxygen of the hydroxamate moiety showed to be of average stability with persistence of 68%. Same observations about the other hydrogen bond interactions during the simulation in the short

runs could be made. The hydrogen bond interaction between the oxygen of the methoxy group in the ortho position to the hydroxamate moiety and Tyr304 demonstrated persistence of 85%, while for His183, a weakly stable hydrogen bond with the carbonyl of the amide linker showing persistence of 42% could be observed. Overall, the predicted binding mode of the hit compound demonstrated good stability during the MD simulation. The key interactions of the zinc binding group were not affected by the slight shift of the ligand from the initial docked pose or the fluctuation of the capping group (**Fig. 10 and 11**).
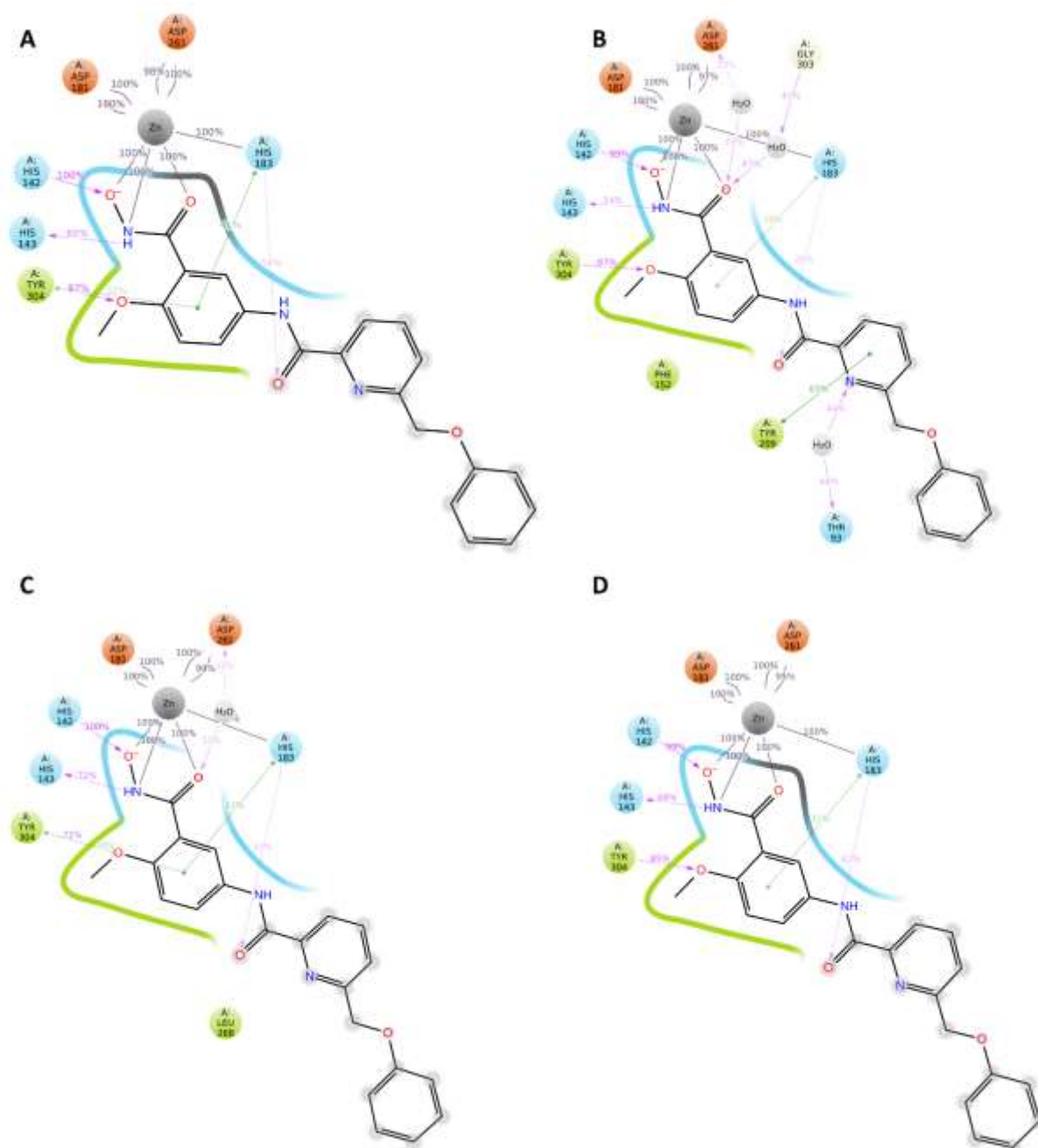
**Fig. 10A, B, C and D**. Ligand interaction persistence diagram for the three independent short MD runs (50 ns) and the long MD run (500 ns) of HDAC11- ZINC000028464438 (**1**).
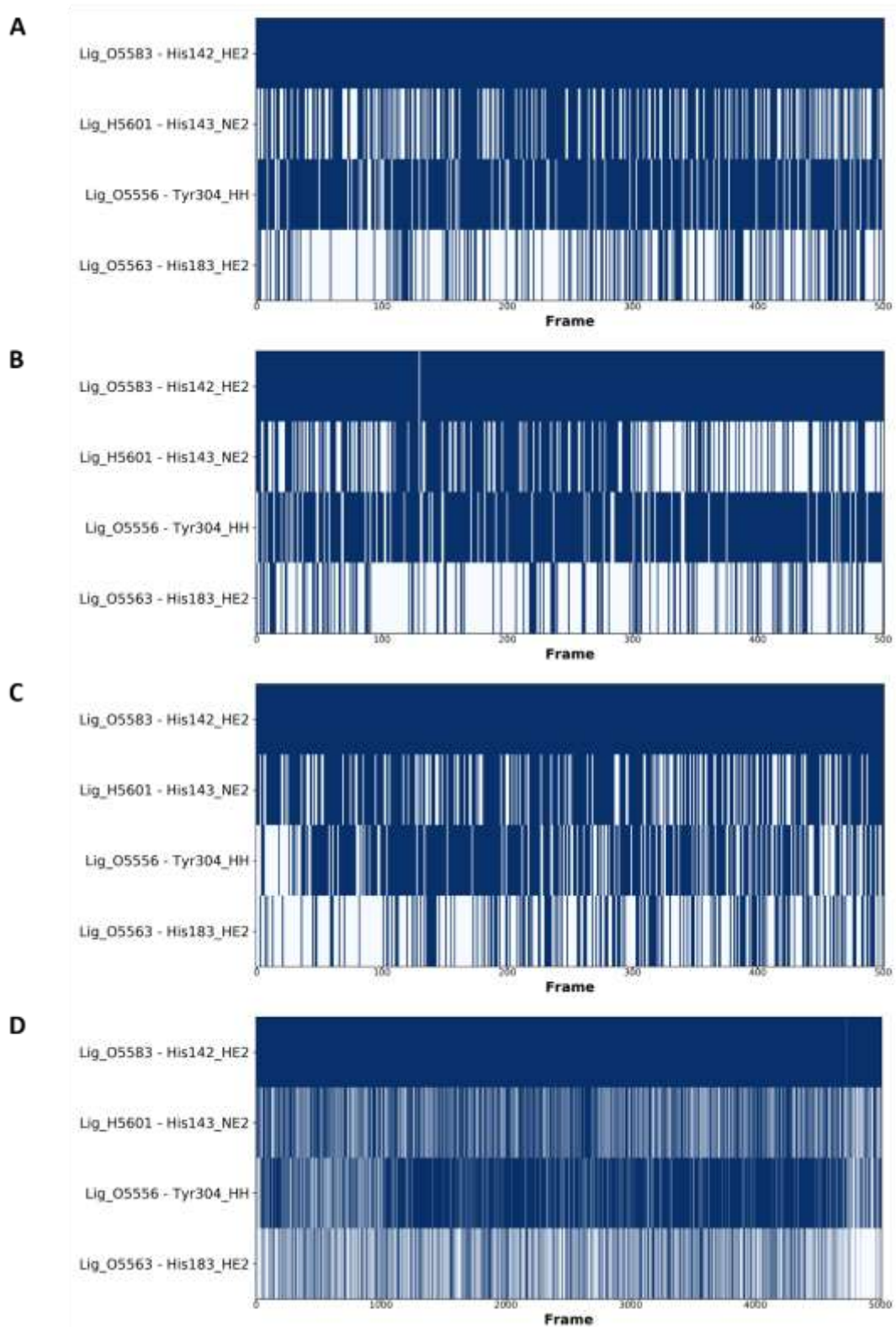
**Fig. 11A, B, C and D. H**ydrogen bond occupancy diagrams for the three independent short MD runs (50 ns) and the long MD run (500 ns), respectively of HDAC11- ZINC000028464438 (**1**).

## 4-Conclusion:

In the current study a structure-based pharmacophore model utilizing our previously optimized HDAC11 AlphaFold model was implemented as preliminary step for screening a large, focused library of benzohydroxamate compounds. The resulted hits were further docked in HDAC11 model and followed by pose filtration to select compounds that could show bidentate chelation of the catalytic zinc ion. A comparative approach was then applied by screening the hits obtained from docking in HDAC11 using different selected HDAC isoform (HDAC1, HDAC6 and HDAC8) crystal structures and eliminating compounds that showed good poses in other HDAC isoforms. This approach proved effective in filtering the initially obtained hit compounds to find a selective ligand. The obtained hits that could show good poses in HDAC11 but not in the other isoforms were subjected to a final filtration step using REOS filter and the final hits were further prioritized by MM-GBSA calculations.  It is interesting to see that all top-ranked hits have a substituent in ortho-position to the aromatic hydroxamate group. This ortho-substituent is sterically accepted in the HDAC11 binding pocket only. In all other HDAC structures studied in the current work this substitution leads to the abolition of the correct chelation of the zinc ion. The experimentally confirmed selectivity for HDAC11 underpins the usefulness of the optimized HDAC11 AlphaFold model for structure-based drug design.

Moreover, the binding mode of the confirmed hit in HDAC11 was further analyzed by several MD simulations. MD simulation studies proved the stability of the initially observed binding mode in terms of ligand RMSD, RMSF, bidentate chelation of the zinc ion and interaction stability.

As a conclusion, a multistep and comparative virtual screening approach was successfully implemented in an attempt to identify novel selective HDAC11 inhibitors utilizing a previously optimized HDAC11 AlphaFold model. This study verifies experimentally the HDAC11 AlphaFold model optimization approach we adopted in our previous study. Additionally, it also confirms that AlphaFold models can be utilized for the aim of drug design and discovery subsequent to a prior optimization.

## Supplementary Materials:

The following supporting information can be downloaded at XXX: Details on the chemical synthesis and analytical characterization as well as details on the hit selection process.

## Author Contributions:

FB did the computational studies, synthesized the compound and and wrote the manuscript. D. R. supervised the computational studies and wrote part of the manuscript. M. Z. performed the HDAC in

vitro testing of the hit compound. C.B. expressed the HDAC11 protein for in vitro testing. M.S. and WS supervised the experiments and revised the manuscript.

## Acknowledgements:

Conflicts of Interest: The authors declare no conflict of interest

### References:

1.    Liu, S.-S., F. Wu, Y.-M. Jin, W.-Q. Chang, and T.-M. Xu, *HDAC11: a rising star in epigenetics.* Biomedicine & Pharmacotherapy, 2020. **131**: p. 110607.

2.    Gao, L., M.A. Cueto, F. Asselbergs, and P. Atadja, *Cloning and functional characterization of HDAC11, a novel member of the human histone deacetylase family.* J Biol Chem, 2002. **277**(28): p. 25748-55.

3.    Villagra, A., F. Cheng, H.W. Wang, I. Suarez, M. Glozak, M. Maurin, D. Nguyen, K.L. Wright, P.W. Atadja, K. Bhalla, J. Pinilla-Ibarz, E. Seto, and E.M. Sotomayor, *The histone deacetylase HDAC11 regulates the expression of interleukin 10 and immune tolerance.* Nat Immunol, 2009. **10**(1): p. 92-100.

4.    Yang, H., J. Yang, H. Cheng, H. Cao, S. Tang, Q. Wang, J. Zhao, B. Li, Y. Ding, and C. Ma, *Probiotics ingestion prevents HDAC11-induced DEC205+ dendritic cell dysfunction in night shift nurses.* Sci Rep, 2019. **9**(1): p. 18002.

5.    Yanginlar, C. and C. Logie, *HDAC11 is a regulator of diverse immune functions.* Biochimica et Biophysica Acta (BBA) - Gene Regulatory Mechanisms, 2018. **1861**(1): p. 54-59.

6.    Cao, J., L. Sun, P. Aramsangtienchai, N.A. Spiegelman, X. Zhang, W. Huang, E. Seto, and H. Lin, *HDAC11 regulates type I interferon signaling through defatty-acylation of SHMT2.* Proc Natl Acad Sci U S A, 2019. **116**(12): p. 5487-5492.

7.    Bagchi, R.A., B.S. Ferguson, M.S. Stratton, T. Hu, M.A. Cavasin, L. Sun, Y.H. Lin, D. Liu, P. Londono, K. Song, M.F. Pino, L.M. Sparks, S.R. Smith, P.E. Scherer, S. Collins, E. Seto, and T.A. McKinsey, *HDAC11 suppresses the thermogenic program of adipose tissue via BRD2.* JCI Insight, 2018. **3**(15).

8.  Sun, L., C. Marin de Evsikova, K. Bian, A. Achille, E. Telles, H. Pei, and E. Seto, *Programming and Regulation of Metabolic Homeostasis by HDAC11.* EBioMedicine, 2018. **33**: p. 157-168.

9.  Fei, Q., F. Song, X. Jiang, H. Hong, X. Xu, Z. Jin, X. Zhu, B. Dai, J. Yang, C. Sui, and M. Xu, *LncRNA ST8SIA6-AS1 promotes hepatocellular carcinoma cell proliferation and resistance to apoptosis by targeting miR-4656/HDAC11 axis.* Cancer Cell Int, 2020. **20**: p. 232.

10. Freese, K., T. Seitz, P. Dietrich, S.M.L. Lee, W.E. Thasler, A. Bosserhoff, and C. Hellerbrand, *Histone Deacetylase Expressions in Hepatocellular Carcinoma and Functional Effects of Histone Deacetylase Inhibitors on Liver Cancer Cells In Vitro.* Cancers (Basel), 2019. **11**(10).

11. Gong, D., Z. Zeng, F. Yi, and J. Wu, *Inhibition of histone deacetylase 11 promotes human liver cancer cell apoptosis.* Am J Transl Res, 2019. **11**(2): p. 983-990.

12. Huo, W., F. Qi, and K. Wang, *Long non-coding RNA BCYRN1 promotes prostate cancer progression via elevation of HDAC11.* Oncol Rep, 2020. **44**(3): p. 1233-1245.

13. Wang, W., B. Ding, W. Lou, and S. Lin, *Promoter Hypomethylation and miR-145-5p Downregulation- Mediated HDAC11 Overexpression Promotes Sorafenib Resistance and Metastasis of Hepatocellular Carcinoma Cells.* Front Cell Dev Biol, 2020. **8**: p. 724.

14. Wang, W., L. Fu, S. Li, Z. Xu, and X. Li, *Histone deacetylase 11 suppresses p53 expression in pituitary tumor cells.* Cell Biol Int, 2017. **41**(12): p. 1290-1295.

15. Mithraprabhu, S., A. Kalff, A. Chow, T. Khong, and A. Spencer, *Dysregulated Class I histone deacetylases are indicators of poor prognosis in multiple myeloma.* Epigenetics, 2014. **9**(11): p. 1511-20.

16. Yue, L., V. Sharma, N.P. Horvat, A.A. Akuffo, M.S. Beatty, C. Murdun, C. Colin, J.M.R. Billington, W.E. Goodheart, E. Sahakian, L. Zhang, J.J. Powers, N.E. Amin, Q.T. Lambert-Showers, L.N. Darville, J. Pinilla-Ibarz, G.W. Reuther, K.L. Wright, C. Conti, J.Y. Lee, X. Zheng, P.Y. Ng, M.W. Martin, C.G. Marshall, J.M. Koomen, R.L. Levine, A. Verma, H.L. Grimes, E.M. Sotomayor, Z. Shao, and P.K. Epling-Burnette, *HDAC11 deficiency disrupts oncogene-induced hematopoiesis in myeloproliferative neoplasms.* Blood, 2020. **135**(3): p. 191-207.

17. Thole, T.M., M. Lodrini, J. Fabian, J. Wuenschel, S. Pfeil, T. Hielscher, A. Kopp-Schneider, U. Heinicke, S. Fulda, O. Witt, A. Eggert, M. Fischer, and H.E. Deubzer, *Neuroblastoma cells depend on HDAC11 for mitotic cell cycle progression and survival.* Cell Death Dis, 2017. **8**(3): p. e2635.

18.     Baselious, F., D. Robaa, and W. Sippl, *Utilization of AlphaFold models for drug discovery: Feasibility and challenges. Histone deacetylase 11 as a case study.* Computers in Biology and Medicine, 2023: p. 107700.

19.     Jumper, J., R. Evans, A. Pritzel, T. Green, M. Figurnov, O. Ronneberger, K. Tunyasuvunakool, R. Bates, A. Žídek, A. Potapenko, A. Bridgland, C. Meyer, S.A.A. Kohl, A.J. Ballard, A. Cowie, B. Romera-Paredes, S. Nikolov, R. Jain, J. Adler, T. Back, S. Petersen, D. Reiman, E. Clancy, M. Zielinski, M. Steinegger, M. Pacholska, T. Berghammer, S. Bodenstein, D. Silver, O. Vinyals, A.W. Senior, K. Kavukcuoglu, P. Kohli, and D. Hassabis, *Highly accurate protein structure prediction with AlphaFold.* Nature, 2021. **596**(7873): p. 583-589.

20.     David, A., S. Islam, E. Tankhilevich, and M.J.E. Sternberg, *The AlphaFold Database of Protein Structures: A Biologist's Guide.* J Mol Biol, 2022. **434**(2): p. 167336.

21.     Ren, F., X. Ding, M. Zheng, M. Korzinkin, X. Cai, W. Zhu, A. Mantsyzov, A. Aliper, V. Aladinskiy, Z. Cao, S. Kong, X. Long, B.H. Man Liu, Y. Liu, V. Naumov, A. Shneyderman, I.V. Ozerov, J. Wang, F.W. Pun, D.A. Polykovskiy, C. Sun, M. Levitt, A. Aspuru-Guzik, and A. Zhavoronkov, *AlphaFold accelerates artificial intelligence powered drug discovery: efficient discovery of a novel CDK20 small molecule inhibitor.* Chemical Science, 2023. **14**(6): p. 1443-1452.

22.     Zhu, W., X. Liu, Q. Li, F. Gao, T. Liu, X. Chen, M. Zhang, A. Aliper, F. Ren, X. Ding, and A. Zhavoronkov, *Discovery of novel and selective SIK2 inhibitors by the application of AlphaFold structures and generative models.* Bioorganic & Medicinal Chemistry, 2023. **91**: p. 117414.

23.     Holcomb, M., Y.T. Chang, D.S. Goodsell, and S. Forli, *Evaluation of AlphaFold2 structures as docking targets.* Protein Sci, 2023. **32**(1): p. e4530.

24.     He, X.-h., C.-z. You, H.-l. Jiang, Y. Jiang, H.E. Xu, and X. Cheng, *AlphaFold2 versus experimental structures: evaluation on G protein-coupled receptors.* Acta Pharmacologica Sinica, 2023. **44**(1): p. 1-7.

25.     Lee, S., S. Kim, G.R. Lee, S. Kwon, H. Woo, C. Seok, and H. Park, *Evaluating GPCR modeling and docking strategies in the era of deep learning-based protein structure prediction.* Comput Struct Biotechnol J, 2023. **21**: p. 158-167.

26.     Heo, L. and M. Feig, *Multi-state modeling of G-protein coupled receptors at experimental accuracy.* Proteins, 2022. **90**(11): p. 1873-1885.

27.     Karelina, M., J.J. Noh, and R.O. Dror, *How accurately can one predict drug binding modes using AlphaFold models?* 2023, eLife Sciences Publications, Ltd.

28.     Díaz-Rovira, A.M., H. Martín, T. Beuming, L. Díaz, V. Guallar, and S.S. Ray, *Are Deep Learning Structural Models Sufficiently Accurate for Virtual Screening? Application of Docking Algorithms to AlphaFold2 Predicted Structures.* Journal of Chemical Information and Modeling, 2023. **63**(6): p. 1668-1674.

29.     Scardino, V., J.I. Di Filippo, and C.N. Cavasotto, *How good are AlphaFold models for docking-based virtual screening?* iScience, 2023. **26**(1): p. 105920.

30.     Zhang, Y., M. Vass, D. Shi, E. Abualrous, J.M. Chambers, N. Chopra, C. Higgs, K. Kasavajhala, H. Li, P. Nandekar, H. Sato, E.B. Miller, M.P. Repasky, and S.V. Jerome, *Benchmarking Refined and Unrefined AlphaFold2 Structures for Hit Discovery.* Journal of Chemical Information and Modeling, 2023. **63**(6): p. 1656-1667.

31.     *Schrödinger Release 2019-1: Maestro, Schrödinger, LLC, New York, NY, 2019.*

32.     Sastry, G.M., M. Adzhigirey, T. Day, R. Annabhimoju, and W. Sherman, *Protein and ligand preparation: parameters, protocols, and influence on virtual screening enrichments.* J Comput Aided Mol Des, 2013. **27**(3): p. 221-34.

33.     *Schrödinger Release 2019-1: Protein Preparation Wizard; Epik, Schrödinger, LLC, New York, NY, 2019; Impact, Schrödinger, LLC, New York, NY, 2019; Prime, Schrödinger, LLC, New York, NY, 2019.*

34.     Jacobson, M.P., D.L. Pincus, C.S. Rapp, T.J. Day, B. Honig, D.E. Shaw, and R.A. Friesner, *A hierarchical approach to all-atom protein loop prediction.* Proteins, 2004. **55**(2): p. 351-67.

35.     Jacobson, M.P., R.A. Friesner, Z. Xiang, and B. Honig, *On the role of the crystal environment in determining protein side-chain conformations.* J Mol Biol, 2002. **320**(3): p. 597-608.

36.     *Schrödinger Release 2019-1: Prime, Schrödinger, LLC, New York, NY, 2019.*

37.     Greenwood, J.R., D. Calkins, A.P. Sullivan, and J.C. Shelley, *Towards the comprehensive, rapid, and accurate prediction of the favorable tautomeric states of drug-like molecules in aqueous solution.* J Comput Aided Mol Des, 2010. **24**(6-7): p. 591-604.

38.     Shelley, J.C., A. Cholleti, L.L. Frye, J.R. Greenwood, M.R. Timlin, and M. Uchimaya, *Epik: a software program for pK( a ) prediction and protonation state generation for drug-like molecules.* J Comput Aided Mol Des, 2007. **21**(12): p. 681-91.

39.     *Schrödinger Release 2019-1: Epik, Schrödinger, LLC, New York, NY, 2019.*

40.     *Schrödinger Release 2019-1: LigPrep, Schrödinger, LLC, New York, NY, 2019.*

41.     Irwin, J.J., K.G. Tang, J. Young, C. Dandarchuluun, B.R. Wong, M. Khurelbaatar, Y.S. Moroz, J. Mayfield, and R.A. Sayle, *ZINC20—A Free Ultralarge-Scale Chemical Database for Ligand Discovery.* Journal of Chemical Information and Modeling, 2020. **60**(12): p. 6065-6073.

42.     Harder, E., W. Damm, J. Maple, C. Wu, M. Reboul, J.Y. Xiang, L. Wang, D. Lupyan, M.K. Dahlgren, J.L. Knight, J.W. Kaus, D.S. Cerutti, G. Krilov, W.L. Jorgensen, R. Abel, and R.A. Friesner, *OPLS3: A Force Field Providing Broad Coverage of Drug-like Small Molecules and Proteins.* J Chem Theory Comput, 2016. **12**(1): p. 281-96.

43.     Shivakumar, D., J. Williams, Y. Wu, W. Damm, J. Shelley, and W. Sherman, *Prediction of Absolute Solvation Free Energies using Molecular Dynamics Free Energy Perturbation and the OPLS Force Field.* Journal of Chemical Theory and Computation, 2010. **6**(5): p. 1509-1519.

44.     Jorgensen, W.L., D.S. Maxwell, and J. Tirado-Rives, *Development and Testing of the OPLS All-Atom Force Field on Conformational Energetics and Properties of Organic Liquids.* Journal of the American Chemical Society, 1996. **118**(45): p. 11225-11236.

45.     Jorgensen, W.L. and J. Tirado-Rives, *The OPLS [optimized potentials for liquid simulations] potential functions for proteins, energy minimizations for crystals of cyclic peptides and crambin.* Journal of the American Chemical Society, 1988. **110**(6): p. 1657-1666.

46.     *Schrödinger Release 2019-1: QikProp, Schrödinger, LLC, New York, NY, 2019.*

47.     Salam, N.K., R. Nuti, and W. Sherman, *Novel method for generating structure-based pharmacophores using energetic analysis.* J Chem Inf Model, 2009. **49**(10): p. 2356-68.

48.     Loving, K., N.K. Salam, and W. Sherman, *Energetic analysis of fragment docking and application to structure-based pharmacophore hypothesis generation.* J Comput Aided Mol Des, 2009. **23**(8): p. 541-54.

49.     Dixon, S.L., A.M. Smondyrev, E.H. Knoll, S.N. Rao, D.E. Shaw, and R.A. Friesner, *PHASE: a new engine for pharmacophore perception, 3D QSAR model development, and 3D database screening: 1. Methodology and preliminary results.* J Comput Aided Mol Des, 2006. **20**(10-11): p. 647-71.

50.     Dixon, S.L., A.M. Smondyrev, and S.N. Rao, *PHASE: A Novel Approach to Pharmacophore Modeling and 3D Database Searching.* Chemical Biology & Drug Design, 2006. **67**(5): p. 370-372.

51.     *Schrödinger Release 2019-1: Phase, Schrödinger, LLC, New York, NY, 2019.*

52.     Friesner, R.A., R.B. Murphy, M.P. Repasky, L.L. Frye, J.R. Greenwood, T.A. Halgren, P.C. Sanschagrin, and D.T. Mainz, *Extra precision glide: docking and scoring incorporating a model of hydrophobic enclosure for protein-ligand complexes.* J Med Chem, 2006. **49**(21): p. 6177-96.

53.     Friesner, R.A., J.L. Banks, R.B. Murphy, T.A. Halgren, J.J. Klicic, D.T. Mainz, M.P. Repasky, E.H. Knoll, M. Shelley, J.K. Perry, D.E. Shaw, P. Francis, and P.S. Shenkin, *Glide: a new approach for rapid, accurate docking and scoring. 1. Method and assessment of docking accuracy.* J Med Chem, 2004. **47**(7): p. 1739-49.

54.     Halgren, T.A., R.B. Murphy, R.A. Friesner, H.S. Beard, L.L. Frye, W.T. Pollard, and J.L. Banks, *Glide: A New Approach for Rapid, Accurate Docking and Scoring. 2. Enrichment Factors in Database Screening.* Journal of Medicinal Chemistry, 2004. **47**(7): p. 1750-1759.

55.     *Schrödinger Release 2019-1: Glide, Schrödinger, LLC, New York, NY, 2019*.

56.     Duan, J., S.L. Dixon, J.F. Lowrie, and W. Sherman, *Analysis and comparison of 2D fingerprints: insights into database screening performance using eight fingerprint methods.* J Mol Graph Model, 2010. **29**(2): p. 157-70.

57.     Sastry, M., J.F. Lowrie, S.L. Dixon, and W. Sherman, *Large-Scale Systematic Analysis of 2D Fingerprint Methods and Parameters to Improve Virtual Screening Enrichments.* Journal of Chemical Information and Modeling, 2010. **50**(5): p. 771-784.

58.     *Schrödinger Release 2019-1: Canvas, Schrödinger, LLC, New York, NY, 2019*.

59.     Bowers, K.J., D.E. Chow, H. Xu, R.O. Dror, M.P. Eastwood, B.A. Gregersen, J.L. Klepeis, I. Kolossvary, M.A. Moraes, F.D. Sacerdoti, J.K. Salmon, Y. Shan, and D.E. Shaw. *Scalable Algorithms for Molecular Dynamics Simulations on Commodity Clusters*. in *SC '06: Proceedings of the 2006 ACM/IEEE Conference on Supercomputing*. 2006.

60.     *Schrödinger Release 2019-1; Desmond Molecular Dynamics System, D.E. Shaw Research: New York, NY, USA, 2019; Maestro-Desmond Interoperability Tools, Schrödinger: New York, NY, USA, 2019*.

61.     Kutil, Z., Z. Novakova, M. Meleshin, J. Mikesova, M. Schutkowski, and C. Barinka, *Histone Deacetylase 11 Is a Fatty-Acid Deacylase.* ACS Chemical Biology, 2018. **13**(3): p. 685-693.

62.     Zessin, M., Z. Kutil, M. Meleshin, Z. Nováková, E. Ghazy, D. Kalbas, M. Marek, C. Romier, W. Sippl, C. Bařinka, and M. Schutkowski, *One-Atom Substitution Enables Direct and Continuous Monitoring of Histone Deacylase Activity.* Biochemistry, 2019. **58**(48): p. 4777-4789.

63. Heimburg, T., F.R. Kolbinger, P. Zeyen, E. Ghazy, D. Herp, K. Schmidtkunz, J. Melesina, T.B. Shaik, F. Erdmann, M. Schmidt, C. Romier, D. Robaa, O. Witt, I. Oehme, M. Jung, and W. Sippl, *Structure-Based Design and Biological Characterization of Selective Histone Deacetylase 8 (HDAC8) Inhibitors with Anti-Neuroblastoma Activity.* Journal of Medicinal Chemistry, 2017. **60**(24): p. 10188-10204.

64. Zhang, L., J. Zhang, Q. Jiang, L. Zhang, and W. Song, *Zinc binding groups for histone deacetylase inhibitors.* J Enzyme Inhib Med Chem, 2018. **33**(1): p. 714-721.

65. De Vreese, R. and M. D'Hooghe, *Synthesis and applications of benzohydroxamic acid-based histone deacetylase inhibitors.* Eur J Med Chem, 2017. **135**: p. 174-195.

66. Hu, Z., F. Wei, Y. Su, Y. Wang, Y. Shen, Y. Fang, J. Ding, and Y. Chen, *Histone deacetylase inhibitors promote breast cancer metastasis by elevating NEDD9 expression.* Signal Transduction and Targeted Therapy, 2023. **8**(1): p. 11.

67. Lipinski, C.A., F. Lombardo, B.W. Dominy, and P.J. Feeney, *Experimental and computational approaches to estimate solubility and permeability in drug discovery and development settings.* Adv Drug Deliv Rev, 2001. **46**(1-3): p. 3-26.

68. Kumari, S., S. Chakraborty, M. Ahmad, V. Kumar, P.B. Tailor, and B.K. Biswal, *Identification of probable inhibitors for the DNA polymerase of the Monkeypox virus through the virtual screening approach.* Int J Biol Macromol, 2023. **229**: p. 515-528.

69. Walters, W.P., M.T. Stahl, and M.A. Murcko, *Virtual screening—an overview.* Drug Discovery Today, 1998. **3**(4): p. 160-178.

70. Walters, W.P. and M. Namchuk, *Designing screens: how to make your hits a hit.* Nat Rev Drug Discov, 2003. **2**(4): p. 259-66.

71. Bai, P., Y. Liu, L. Yang, W. Ding, P. Mondal, N. Sang, G. Liu, X. Lu, T.T. Ho, Y. Zhou, R. Wu, V.C. Birar, M.Q. Wilks, R.E. Tanzi, H. Lin, C. Zhang, W. Li, S. Shen, and C. Wang, *Development and Pharmacochemical Characterization Discover a Novel Brain-Permeable HDAC11-Selective Inhibitor with Therapeutic Potential by Regulating Neuroinflammation in Mice.* Journal of Medicinal Chemistry, 2023.

72. Dan, A., T. Shiyama, K. Yamazaki, N. Kusunose, K. Fujita, H. Sato, K. Matsui, and M. Kitano, *Discovery of hydroxamic acid analogs as dual inhibitors of phosphodiesterase-1 and -5.* Bioorg Med Chem Lett, 2005. **15**(18): p. 4085-90.